



A numerical investigation of fluid flow path evolution during cataclastic flow in reservoir rocks

KAMAL NANDA¹, SUAIBA MUFTI¹, ARGHYA DAS^{1,*}  and SANTANU MISRA²

¹Department of Civil Engineering, Indian Institute Technology Kanpur, Kanpur 208 016, India.

²Department of Earth Sciences, Indian Institute Technology Kanpur, Kanpur 208 016, India.

*Corresponding author. e-mail: arghya@iitk.ac.in

MS received 17 May 2023; revised 31 August 2023; accepted 18 September 2023

We simulate cataclastic flow deformation using discrete elements for high porous Bentheim sandstone under 1D compression and high confinement (~ 300 MPa) to assess the flow path and permeability evolution during cataclasis. The model accounts for particle crushing by replacing balls with smaller fragments and cement damage by removing existing bonds beyond a threshold stress level. The particle packing in the deformed numerical specimens is further analysed using an image processing tool to extract the pore structure. The analysis suggests that beyond 10% particle breakage, there is a decreasing trend in tortuosity, indicating the crushed finer fragments enable additional flow channels. The same is quantitatively ascertained through pore coordination number and visual identification. The overall analysis implies that during the compression under high confinement, the rate of permeability reduction depends on the flow path evolution due to crushing, and tortuosity can decrease due to excessive crushing.

Keywords. Tortuosity; cataclastic flow; porous rock; particle crushing; discrete element method.

1. Introduction

Experimental studies over the last three decades on porous granular rocks (e.g., sandstone and limestone) demonstrate failure by cataclastic flow (matrix-controlled cataclasis) at the brittle and brittle–ductile transitions (Wong and Baud 2012; Leuthold *et al.* 2021a; Sari *et al.* 2022). Under high confinement (>150 MPa) and depending on the initial porosity, grain size distributions, type of grain bonding cement and effective confining pressures, three different macroscopic failure modes are documented: (i) shear localization, (ii) compaction localization, and (iii) cataclastic compaction (Fortin *et al.* 2009). However, the grain scale microscopic analysis indicates such failure

modes are primarily associated with extensive grain crushing and cement debonding accompanied by pore collapse due to fragment reorganization, which results in porosity reduction (Menéndez *et al.* 1996) and eventually alters the characteristic permeability. In a recent study, Leuthold *et al.* (2021a) reported a three-fold reduction in permeability in carbonate rock due to 40% axial compression. Analysis of simultaneous cataclastic flow failure and permeability evolution is, therefore, of great importance in various practical applications like hydro-mechanical coupling in porous reservoir rocks, aquifer management, seafloor subsidence, tectonic activity, and borehole stability in porous rock (Fossen *et al.* 2007; Fortin *et al.* 2009; Lee *et al.* 2016).

However, permeability evolution due to cataclastic flow is non-trivial. It often depends on the three macroscopic failure modes and the microscopic changes due to grain crushing. Zhu and Wong (1997) captured permeability evolution during the brittle–ductile transition on a series of porous sandstones. The experimental analysis showed that permeability reduces with increasing mean effective stress before yielding strength, whereas the deviatoric stress strongly influences permeability evolution after yielding. Vajdova *et al.* (2004) demonstrated a comprehensive experimental analysis that shows permeability evolution at variable rates during compaction localization in high-porosity Bentheim sandstone. Initially, the permeability reduction rate is slow due to elastic compression, then sharply decreases during localized deformation involving pore collapse and crushing. Finally, the rate is further reduced during cataclastic flow regime characterized by significant crushing. Such a distinct zonation may only be observed in some sandstones (e.g., Bentheim at 250 MPa or more confinement and Berea at 160 MPa or more confinement) since the crushing and pore collapse vary with rocks and their intrinsic properties. For instance, high porous sandstones like Boise, Rothback, Adamswiller, and Darley Dale do not show varying rates of permeability reduction in the inelastic deformation, as they lack discrete localized deformation, such as, compaction band and/or shear band development (Zhu and Wong 1997; Baud *et al.* 2006). A recent study on permeability evolution in weakly consolidated sandstone under different stress paths indicates iso-permeability contours coincide with the mechanical yield surface during homogeneous deformation (Nguyen *et al.* 2014). A few studies also indicate the development of anisotropic permeability due to granular fabric orientation during cataclastic flow (Baud *et al.* 2012).

Experimental studies reveal that permeability evolves (reduces, mostly) in high porous sandstones at different rates under different stages of deformation during the brittle–ductile transition (Morris *et al.* 2003; Vajdova *et al.* 2004). However, it is not trivial to anticipate such permeability evolution, especially in the cataclastic flow regime. Advanced constitutive models are efficient in evaluating the deformation response of rock (Issen and Rudnicki 2001; Nguyen and Einav 2009; Das *et al.* 2014). To predict the permeability evolution, either power-law porosity (David *et al.* 1994) or Kozeny-Carman type formulations, accounting for

both porosity and grain crushing (Nguyen and Einav 2009; Esna Ashari *et al.* 2018; Nanda *et al.* 2020; Leuthold *et al.* 2021b), is used. Theoretical analysis mainly uses empirical tortuosity equations, which are inadequate in many cases for quantitative estimation of permeability during post-yielding and post-localized deformation phases despite knowing the porosity and grain breakage information. Also, limited microstructural analysis can predict the tortuosity evolution at the cataclastic flow regime. Hence, the present study aims to bridge the research gap by capturing tortuosity evolution at different stages of cataclastic flow.

The present study clubs the discrete element method (DEM) based on simulated cataclastic rock deformation and pore network model to understand the micromechanics behind permeability evolution. In discrete element simulations, particle crushing is implemented along with grain rearrangement to predict the pore structure realistically. The microscale parameters for the simulation are calibrated based on the laboratory-scale rock deformation data. Later, the pore network is extracted to identify the fluid flow path. Finally, the analysis illustrates the crushing effects on the pore structure evolution and consequent permeability change.

2. Methodology

2.1 Background of analysis

In a recent study, Nanda *et al.* (2020) numerically simulated the fluid flow through porous granular rock, deformed at the brittle–ductile transition regime using finite element method (FEM). Figure 1(a) demonstrates the hydro-mechanical response (porosity and permeability evolution) of Bentheim sandstone undergoing localized compaction due to triaxial compression at 300 MPa confinement. Locally at the integration point, fluid conductance is modelled with the help of the Kozeny-Carman type permeability model (k , equation 1). Despite quantitatively matching the porosity (ϕ) evolution with the experimental observation (Vajdova *et al.* 2004), the permeability of the deformed rock specimen only qualitatively agreed with the experimental data (figure 1a), especially in Zone 3. Nonetheless, the model captures the initial elastic compression-induced permeability reduction (Zone 1) and rapid reduction

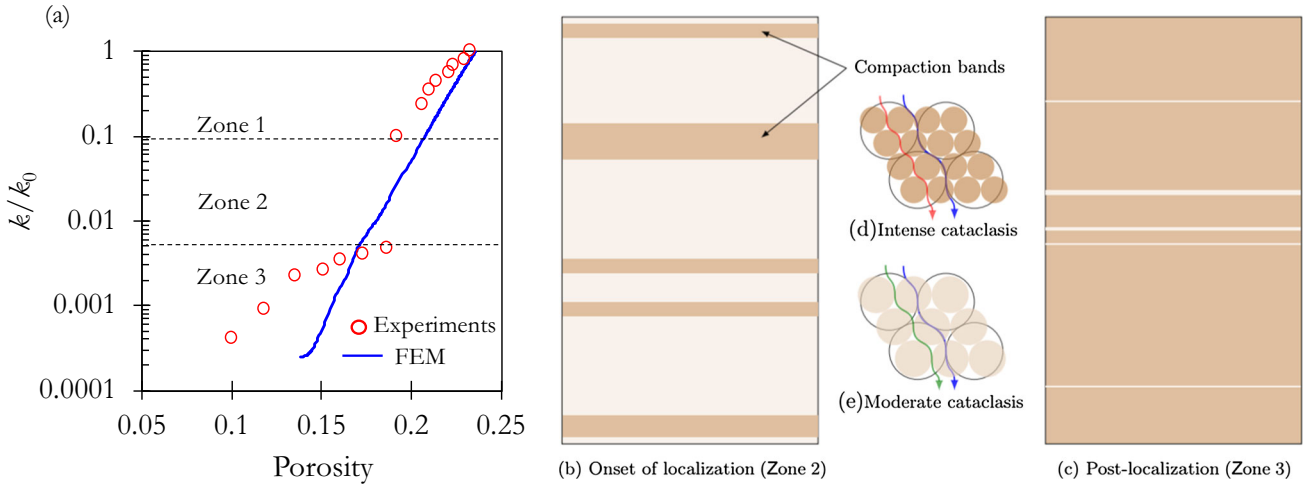


Figure 1. (a) Comparison of permeability variation with porosity reduction due to triaxial compression in Bentheim sandstone at 300 MPa confinement obtained through FE simulation and the experimental observation of Vajdova *et al.* (2004) under similar conditions. (b–e) Different deformation zones and corresponding flow path variations, discussed in the text, are also highlighted.

in permeability during cataclastic flow due to the combined effect of particle breakage and porosity (Zone 2). It can be summarized in two competing mechanisms: (1) permeability reduction due to pore shrinkage and collapse, and (2) tortuosity reduction due to the generation of new flow paths via extension crack in grain scale. A typical schematic of bulk tortuosity variation from the localized zone to the post-localized zone is presented in figure 1(b–e). It can be speculated that in the localization stage, grain comminution is spatially localized in band regions, causing low tortuosity due to crushing relative to outside the band, but bulk tortuosity is relatively high due to significant spatial flow regions outside the bands, materializing sudden drop in permeability. The same is not the case near the ductile regime, where significant (spatially) flow happens in low tortuosity. Therefore, the relative drop in permeability is hindered.

Experimental results show one order of magnitude permeability reduction in Zone 3 (figure 1) with porosity reduction from 18 to 12%. Such a permeability reduction rate is notably slower than in Zone 2. However, FEM analysis using the Kozeny-Carman formulation (equation 1) predicts a similar rate of permeability reduction in Zone 2 and Zone 3 with the increase of specific surface area (S) due to crushing of particles. Such an anomaly between the experimental observation and theoretical prediction indicates that other mechanisms must enhance fluid flow, gradually reducing permeability in the cataclastic flow regime (Zone 3). The deformation in this regime demonstrates a

fully compacted rock sample with closely spaced multiple compaction zones across the sample. A possible explanation could be the evolution of fluid flow path or tortuosity (T), which is generally assumed proportional to porosity and also has grain breakage dependency.

$$k = C_0 \frac{\varphi^3}{T^2 S^2}, \quad (1)$$

$$T = \frac{L_h}{L} = f(\varphi). \quad (2)$$

Fluid flow modelling using finite elements or other continuum approaches requires a permeability model like Kozeny-Carman, along with supplementary assumptions to account for alterations in flow due to microstructural changes. Validation of those assumptions is not trivial. On the contrary, fluid flow analysis based on the pore network obtained from DEM inherently incorporates all pore-scale mechanisms and microstructural changes. Note that DEM-based fluid flow models are useful to validate the assumptions of continuum models for further large-scale simulations. Hence, a microstructural analysis using DEM is presented in the next segment to explore the grain breakage effect on the flow path variation.

2.2 Discrete element model

Numerical studies on permeability evolution in porous granular rock using DEM along with flow

simulation, either Lattice Boltzmann methods (LBM) (Sun *et al.* 2013) or pore network analysis (Wang *et al.* 2021) focus on the dilative deformation zone under low confinement. In experiments, cataclastic flow failure is primarily analyzed using a triaxial compression test at high confining conditions (Menéndez *et al.* 1996). Achieving the same in DEM is challenging since appropriate porosity reduction through simulating pore collapse and particle breakage while maintaining a servo-controlled confining condition is not trivial. An alternative approach is a 1D compression, which does not require servo-controlled lateral confinement (Arroyo *et al.* 2005; Marketos and Bolton 2009) yet leads to cataclastic flow and compaction localization. In addition, continuous compression ensures porosity reduction. The stress trajectory in a 1D compression test is substantiated by the compaction band research as it prompts compaction bands via inducing pore collapse readily. Furthermore, Das *et al.* (2013) and Das and Buscarnera (2014) have shown that the stress path inside the compaction regime closely resembles a 1D compression test.

Parameter calibration. In order to achieve matrix-controlled cataclastic deformation, the grain scale parameters (contact stiffness, cement bond strength and particle crushing strength) of DEM are calibrated (table 1) based on the triaxial experimental on high porosity (25%) Bentheim sandstone (Klein *et al.* 2001). Calibrating the contact parameters in DEM is not straightforward since direct experimental tools are not readily available. Therefore, the calibration requires indirect macroscopic measurement, such as, stress–strain response, mineralogical information, grain size distribution, etc. For example, in the present study, (i) cement bond stiffnesses are obtained from the initial elastic

response of triaxial compression tests; (ii) cement bond strengths are obtained from peak compressive strength at low confining pressure; and (iii) grain fracture or grain breakage parameters are obtained from the threshold of isotropic compression tests. Finally, ball contact stiffnesses are assumed to be similar in the range of bond stiffness, although they are less sensitive to the simulation of bonded granular assemblies. The simulated cylindrical rock specimen (diameter 1 mm and height 2 mm) consists of 15,437 spherical particles, which are prepared in Particle Flow Code 3D, a commercial DEM package (PFC 5). Particle size distribution, available in Cheung *et al.* (2012) for Bentheim sandstone, is used for DEM sample preparation (figure 2a). Intergranular cement bond strength is obtained from the triaxial compression at 10 MPa, assuming bond failure is the primary deformation mechanism under lower confinement (figure 2b). In contrast, the particle crushing strength is estimated by comparing the mean stress evolution under hydrostatic compression (figure 2c). Particle crushing simulation follows the replacement method (Ben-Nun and Einav 2010). In this method, a parent particle is replaced with eight fragments arranged in Apollonian packing (figure 1d) once a contact force-based particle breakage criterion is satisfied. The criteria consider grain size-dependent crushing with Weibull statistical particle survival strategy such that a parent particle undergoes crushing once the average contact normal force exceeds $F_c(d/d_0)^{2-(\frac{3}{w})}$. Here, d_0 is the mean particle diameter, w represents Weibull modulus and F_c is the critical normal load for d_0 . The mass (and volume) of the replaced particles is conserved by gradually increasing the size of the generated fragments in multiple steps after the replacement. An interval is maintained between two successive crushing events in order to minimize any

Table 1. DEM parameters.

Parameters	Value
Density of the particles (kg/m ³)	2650
Particle diameter range (mm)	0.2–0.02
Initial porosity	0.25
The initial number of particles	15437 (UCS/isotropic compression) and 32487 (1D compression)
Normal and shear stiffness (N/m)	5×10^6 and 2×10^7
Inter-particle friction coefficient	0.35
Bond (normal/shear) stiffness (N/m ³)	0.7×10^{15} and 2.8×10^{15}
Parallel bond strength, normal/shear (Pa)	4.5×10^8 and 14×10^8
Critical crushing load (N)	27

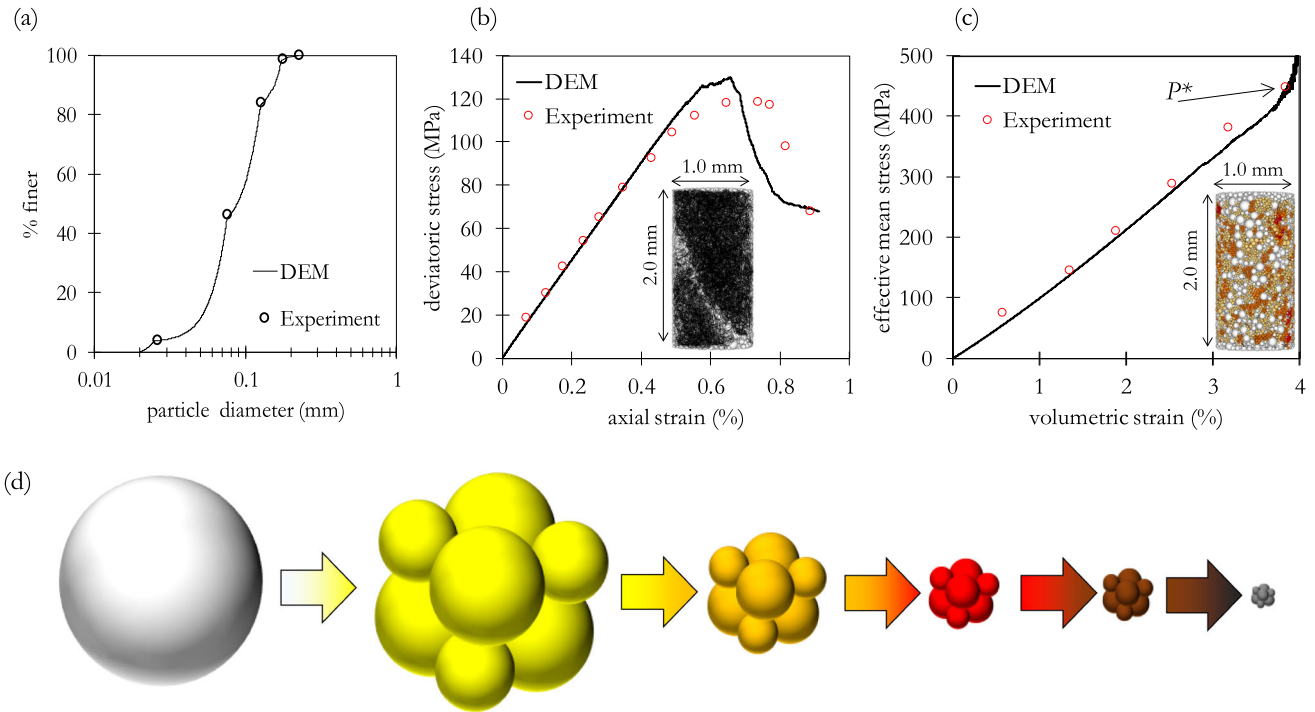


Figure 2. Comparison of DEM and experimental (Klein *et al.* 2001) observation, (a) grain size distribution of Bentheim sandstone; (b) triaxial compression response at low confinement compression, 10 MPa confinement; the black regions in the specimen indicate intact grain bonding cement, while the white region is broken bond which highlights the formation of a shear crack; (c) hydrostatic compression. The coloured particles in the hydrostatically deformed sample indicate different generation of crushing; and (d) relative dimensions of broken fragments in Apollonian packing with colour indicating the breakage generation.

unwanted overlapping contact force that arises due to particle enlargement. A detailed procedure can be found in Das *et al.* (2022) and Bisht and Das (2021). Note that the adopted grain replacement process ignores fine fragments since the theoretical analysis by Esna Ashari *et al.* (2018) demonstrated that accounting fines for the permeability estimation underestimate the results in the cataclastic flow regime. The final comparison between the experiment and simulation shows reasonable agreement that approves the reliability and validity of model calibration and its various assumptions. The observed discrepancy between the experimental result and numerical simulation in the post-peak response under low confinement (figure 2b) can be attributed to the use of rigid boundaries in DEM. In actual rock deformation experiments, flexible jackets are used to confine the rock specimen. This setup allows the sliding of rock blocks along the shear crack (figure 2b), resulting in an instantaneous drop in stress. In DEM simulation, the use of rigid boundary arrests the sliding along the developed crack in the post-peak deformation.

1D compression. In DEM simulation, a cubic sample of $1.5 \times 1.5 \times 1.5$ mm has been prepared

with bonded particle assembly using 32487 discrete spherical solid balls. The numerical specimen is compressed from the top at a constant displacement rate, while the remaining side and bottom boundaries are stationary. Controlling the boundary conditions in cubic specimens is relatively more straightforward, and there is no pressure boundary constraint in 1D compression, unlike the triaxial experiments. Hence, a cube-shaped specimen is chosen. The particle size distribution in the cube is shown in figure 2(a). The stress path during 1D compression of the cube is shown in figure 3(a). The yielding stress points observed in the experiments on Bentheim sandstone are also superimposed on the same plot. The simulation results indicate that the stress path enters the inelastic zone at the brittle–ductile transitional stress state (mean stress 325 MPa and deviatoric stress 175 MPa, the yellow patch zone in figure 3a), where cataclastic flow is expected. The deviatoric stress also shows a trend (figure 3b) similar to that observed by Arroyo *et al.* (2005) in calcarenite subjected to 1D compression. Besides, a series of incrementally compressed (1D) samples display that the particle crushing initiates around 3.0%

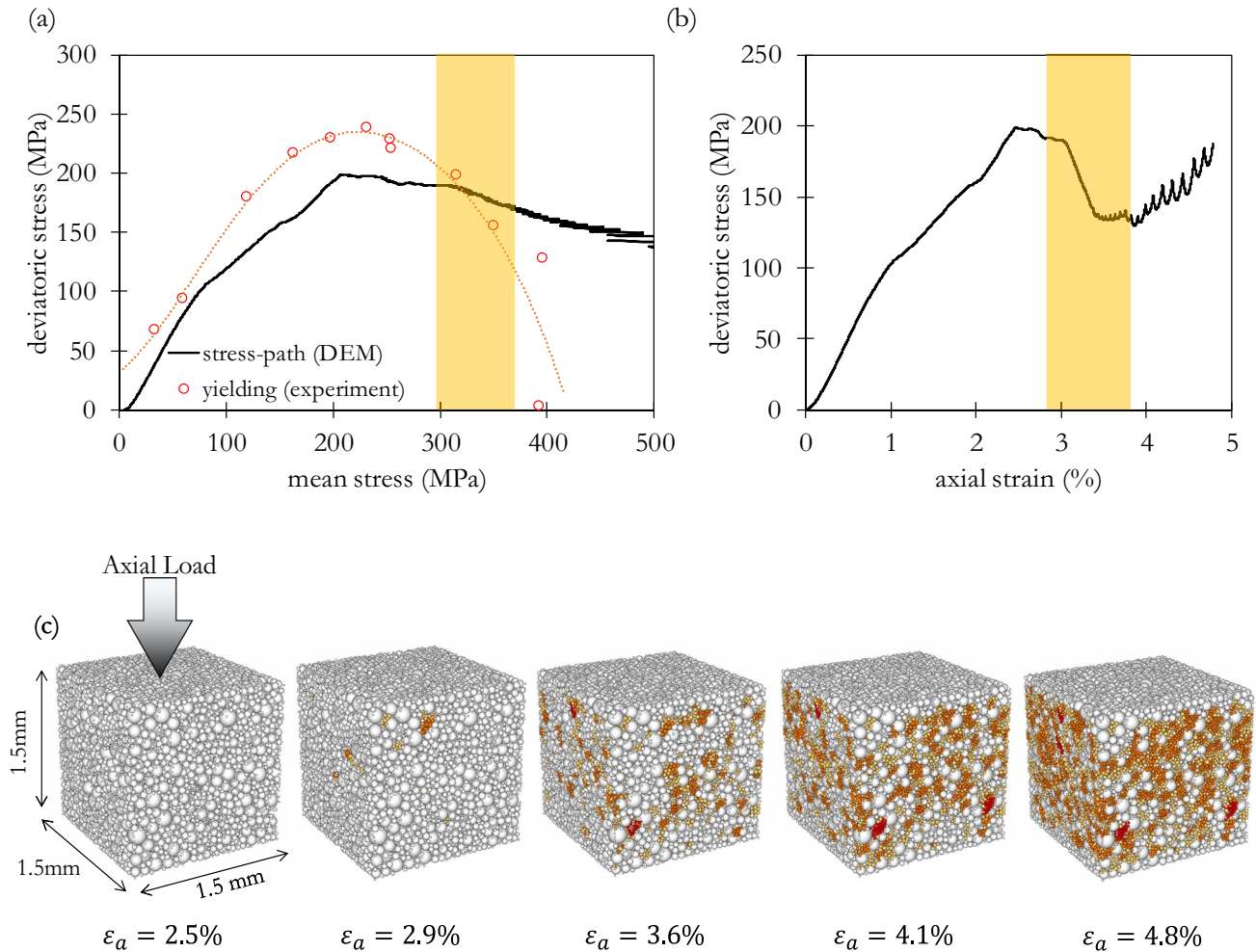


Figure 3. DEM simulation of 1D compression, (a) stress path and experimental yielding surface while highlighting the cataclastic flow zone; (b) deviatoric stress evolution; yellow patch highlights the cataclastic flow regime; (c) deformed DEM specimens at different states of compression. The coloured particles refer to different generation of crushing, as elaborated in figure 2(d).

axial strain (figure 3c), corresponding to the brittle–ductile transitional regime (figure 3b). In the present study, simulation is performed up to 4.8% axial deformation since further compression would increase the number of crushed fragments in manifold and consequently increase the computational cost of DEM.

3. Results and discussion on the flow analysis

To compute the evolution of flow path in the brittle–ductile transitional regime because of pore collapse and particle crushing, we considered tortuosity as the controlling parameter in our analysis. Tortuosity, a ratio between the shortest length of winding fluid flow path at the pore scale to the straight-line distance along the flow direction at

the sample scale, quantitatively assesses the flow path in porous media (Clennell 1997). Conventionally, tortuosity is expressed as a function of porosity alone without considering other microstructural alterations (equation 3, Bruggeman 1935).

$$T^2 = \varphi^{1-\alpha_1}. \quad (3)$$

The power term α_1 in equation (3) quantifies the formation factor for any porous media (Archie 1942).

The assembly of spheres generated in DEM is further analysed in a commercial image processing package (FEI Avizo 2017) to compute the flow path variation due to cataclastic flow deformation. The assembly is first converted into a 3D binarized image, which is then used for estimating the tortuosity of the sample. Tortuosity calculation

requires discretization of void space into pores and throats. Darcy’s law is invoked to calculate the velocity of the fluid in each throat. Finally, tortuosity (along the flow direction) is computed using:

$$T = \frac{\sum_{i=0}^m \|v_i\|}{\sum_{i=0}^m \|vx_i\|}, \quad (4)$$

where m represents the total number of throats, v_i is the velocity of fluid passing through each pore-throat, and vx_i represents the projection of the velocity along the direction of fluid flow passing through the pore-throat i .

The analysis measures tortuosity along the compressive stress direction, which also corresponds to the fluid flow direction through the pore network. Tortuosity can be different in two mutually perpendicular directions provided the deformation is localized in nature and/or the particles are angular in shape to provide the preferred flow direction. In the present study, the observed deformation is homogeneous all through since the cubic specimen only focuses on a local compaction zone. In addition, given the use of spherical particles, it is unlikely to obtain significantly different tortuosity, when measured along the mutually perpendicular directions.

Figure 4(a) compares the analytical (equation 3) and numerical tortuosity (from the DEM using equation 4) predictions with porosity reduction during 1D compression. In addition, the geometric tortuosity evolution in another porous rock, Fontainebleau sandstone (Fu *et al.* 2021), is added to the same plot for comparison. The comparison highlights that the numerical estimation from DEM assembly follows the same trend as analytical results till $\phi = 0.23$, where only elastic deformation is predicted. Interestingly, in the brittle–ductile transition, a sharp increase followed by tortuosity reduction is captured (marked by arrowhead in figure 4a). Besides the numerical analysis, the cross-sections of deformed DEM specimens are captured at different axial strain levels during the compression, and typical flow paths are visually identified. The observed changes in flow path (marked manually with a white line in figure 4c) qualitatively agree with the numerically predicted trend of tortuosity reduction. The length of the flow path reduces with increasing compression, indicating tortuosity drop. The flow paths are initially more winding than the crushed specimens, resulting in a relatively slower flow. Tortuosity variation under different porosity estimated using

LBM simulation on Fontainebleau sandstone (Fu *et al.* 2021) also corroborates with analytical models since only porosity change is considered.

Particle breakage is computed from the evolving grain size distribution at different stages of deformation. In addition, a histogram of pore coordination number is also plotted. For the quantification of particle crushing, relative breakage (B_r) is calculated based on the initial grain size distribution and a fractal-type ultimate distribution proposed by Einav (2007) (figure 5a). The breakage evolution against porosity reduction (figure 5a) demonstrates a sharp increase (10–50%) at $\phi = 0.23$, possibly resulting in the decay in tortuosity by creating additional flow paths. Before the initiation of crushing ($\epsilon_a = 2.9\%$), the modal normalized coordination number was 2.5, which shifts to 4.5 (see figure 5b) with increasing particle crushing during the cataclastic flow at $\epsilon_a = 4.8\%$ indicating a significant increase in the pore connectivity due to crushing that is responsible for the enhancement in permeability. Therefore, the conventional models (e.g., equation 3) that only predict increasing tortuosity with reducing porosity (Matyka *et al.* 2008; Fu *et al.* 2021) cannot be used to determine the hydraulic characteristic in complex deformation processes like cataclasis.

The rate of reduction in permeability largely depends on the effect of individual localization band formation, a relationship that has been previously established experimentally (Baud *et al.* 2004) and numerically (Nanda *et al.* 2020). Therefore, the present study (1D compression) explores the local hydro-mechanical response within a localized compaction zone. This local response has a direct influence on the overall permeability reduction when such multiple discrete compaction zones emerge in the Bentheim sandstone. Once multiple such discrete compaction zones are formed in a bigger cylindrical sandstone specimen under triaxial compression loading, the overall permeability reduction rate drastically reduces, as noticed in experiments. Nonetheless, we do not quantify the reservoir scale permeability in the present study but demonstrate the local flow mechanisms during cataclastic deformation.

The present DEM simulation does not consider the particle shape effect on the deformation and fluid flow path of porous rock for the sake of simplicity. Particle shape can alter the fluid flow path and tortuosity. However, with multiple generations of crushing events, the shape of the fine fragments approaches a rounded/sub-rounded one (Bisht and Das 2021), which corroborates with the present

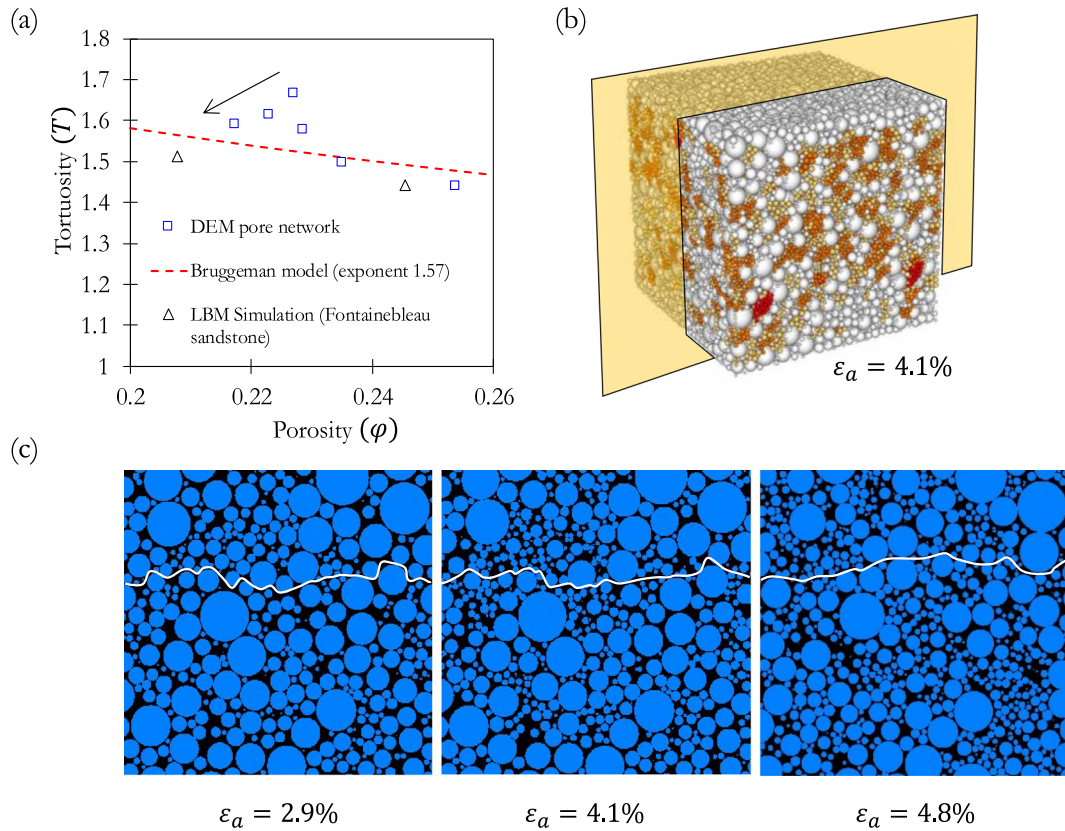


Figure 4. Tortuosity evolution during 1D compression, (a) tortuosity *vs.* porosity plot. The arrow mark indicates reduction in tortuosity despite porosity reduction. LBM simulation results in Fontainebleau sandstone (Fu *et al.* 2021) highlight tortuosity increase with porosity reduction; (b) typical cross-section of DEM specimen; and (c) schematic representation of flow path variation (marked with white line) in 2D cross-section of DEM specimen at different axial strains.

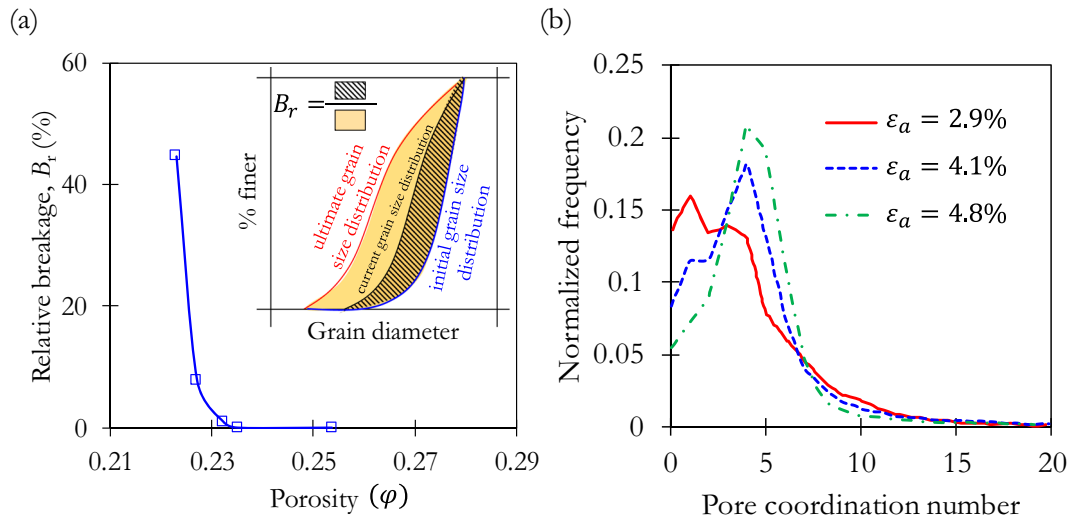


Figure 5. Microstructural changes during cataclastic flow under 1D compression, (a) relative breakage evolution. The inset figure shows the relative breakage definition proposed by Einav (2007); (b) pore-throat coordination number evolution.

modelling assumption of spherical particles. Considering the shape effect in DEM is complex in terms of formulation and computationally expensive once particle crushing is taken into consideration.

4. Conclusions

A DEM-based numerical analysis is proposed to mimic cataclastic flow in granular rock. We explore the evolution of flow path due to pore collapse and

particle crushing during the deformation. The results indicate that tortuosity increases in the elastic deformation and early stages of inelastic deformation due to porosity reduction. However, excessive particle crushing leads to a reduction in tortuosity by creating direct fluid flow paths, which are otherwise winding during the absence of particle crushing. The microstructural analysis demonstrates that 1D compression of 4.8% axial strain results in 40% increases in the relative breakage, which can cause around two times increase in the pore-throat coordination number compared to the elastically deformed sample without any crushing. Based on our results, we finally conclude that in the cataclastic flow regime, porosity reduction due to grain crushing/fragmentation cannot continuously demote the fluid flow as predicted through the conventional analytical models since particle crushing enhances the flow via reducing tortuosity.

Acknowledgements

The authors express their gratitude for the insightful recommendations provided by two anonymous reviewers and for the editorial guidance offered by Prof. Somnath Dasgupta. This work has been supported by SERB grant (No. ECR/2016/001002) and Swarnajayanti Fellowship (No. DST/SJF/E&ASA-01/2015-16) awarded to A Das and S Misra, respectively. K Nanda and S Mufti thank IIT Kanpur for supporting their research. A Das thanks Thermo Fisher Scientific for allowing limited-time use of Avizo-PerGeos tool.

Author statement

Kamal Nanda: Numerical modelling, data analysis, interpretation of results and drafting the original manuscript. Suaiba Mufti: Numerical modelling. Arghya Das: Conceptualisation of work, revision of draft manuscript. Santanu Misra: Revision of draft manuscript and overall support.

References

- Archie G E 1942 The electrical resistivity log as an aid in determining some reservoir characteristics; *Trans. AIME* **146(01)** 54–62.
- Arroyo M, Castellanza R and Nova R 2005 Compaction bands and oedometric testing cemented soils; *Soils Found.* **45(2)** 181–194.
- Baud P, Klein E and Wong T-f 2004 Compaction localization in porous sandstones: Spatial evolution of damage and acoustic emission activity; *J. Struct. Geol.* **26(4)** 603–624, <https://doi.org/10.1016/j.jsg.2003.09.002>.
- Baud P, Vajdova V and Wong T-f 2006 Shear-enhanced compaction and strain localization: Inelastic deformation and constitutive modeling of four porous sandstones; *J. Geophys. Res.* **111(B12)** 1–17, <https://doi.org/10.1029/2005JB004101>.
- Baud P, Meredith P and Townend E 2012 Permeability evolution during triaxial compaction of an anisotropic porous sandstone; *J. Geophys. Res.: Solid Earth* **117(5)**.
- Ben-Nun O and Einav I 2010 The role of self-organization during confined comminution of granular materials; *Phil. Trans. A. Math. Phys. Eng. Sci.* **368** 231–247.
- Bisht M S and Das A 2021 DEM study on particle shape evolution during crushing of granular materials; *Int. J. Geomech.* **21(7)** 04021101.
- Bruggeman D A G 1935 Berechnung verschiedener physikalischer Konstanten von heterogenen Substanzen. I. Dielektrizitätskonstanten und Leitfähigkeiten der Mischkörper aus isotropen Substanzen; *Ann. Phys.* **416(7)** 636–664.
- Cheung C S N, Baud P and Wong T-f 2012 Effect of grain size distribution on the development of compaction localization in porous sandstone; *Geophys. Res. Lett.* **39(21)** 1–5.
- Clennell M Ben 1997 Tortuosity: A guide through the maze; *Geol. Soc. London, Spec. Publ.* **122(1)** 299–344.
- Das A and Buscarnera G 2014 Simulation of localized compaction in high-porosity calcarenite subjected to boundary constraints; *Int. J. Rock Mech. Min. Sci.* **71** 91–104, <https://doi.org/10.1016/j.ijrmms.2014.07.004>.
- Das A, Nguyen G D and Einav I 2013 The propagation of compaction bands in porous rocks based on breakage mechanics; *J. Geophys. Res.: Solid Earth* **118(5)** 2049–2066, <https://doi.org/10.1002/jgrb.50193>.
- Das A, Tengattini A, Nguyen G D, Viggiani G, Hall S A and Einav I 2014 A thermomechanical constitutive model for cemented granular materials with quantifiable internal variables. Part II – Validation and localization analysis; *J. Mech. Phys. Solids* **70** 382–405.
- Das S K, Verma S K and Das A 2022 Numerical assessment of effects of strain rate on the critical state of crushable sand; *Geotech. Lett.* **12(1)** 8–13.
- David C, Wong T-f, Zhu W and Zhang J 1994 Laboratory measurement of compaction-induced permeability change in porous rocks: Implications for the generation and maintenance of pore pressure excess in the crust; *Pure Appl. Geophys.* **143(1–3)** 425–456.
- Einav I 2007 Breakage mechanics – Part I: Theory; *J. Mech. Phys. Solids* **55(6)** 1274–1297.
- Esnah Ashari S, Das A and Buscarnera G 2018 Model-based assessment of the effect of surface area growth on the permeability of granular rocks; *J. Eng. Mech.* **144(5)**.
- FEI Avizo 2017 User's Guide Konrad-Zuse-Zentrum für Informationstechnik Berlin (ZIB); Germany, pp. 940–950.
- Fortin J, Stanchits S, Dresen G and Gueguen Y 2009 Acoustic emissions monitoring during inelastic deformation of porous sandstone: Comparison of three modes of deformation; *Pure Appl. Geophys.* **166(5–7)** 823–841.
- Fossen H, Schultz R A, Shipton Z K and Mair K 2007 Deformation bands in sandstone: A review; *J. Geol. Soc.* **164(4)** 755–769.

- Fu J, Thomas H R and Li C 2021 Tortuosity of porous media: Image analysis and physical simulation; *Earth-Sci. Rev.* **212** 103439.
- Issen K A and Rudnicki J W 2001 Theory of compaction bands in porous rock; *Phys. Chem. Earth, Part A: Solid Earth Geod.* **26(1–2)** 95–100.
- Klein E, Baud P, Reuschlé T and Wong T-f 2001 Mechanical behaviour and failure mode of Bentheim sandstone under triaxial compression; *Phys. Chem. Earth, Part A: Solid Earth Geod.* **26(1–2)** 21–25.
- Lee H, Moon T and Haimson B C 2016 Borehole breakouts induced in Arkosic sandstones and a discrete element analysis; *Rock Mech. Rock Eng.* **49** 1369–1388, <https://doi.org/10.1007/s00603-015-0812-0>.
- Leuthold J, Gerolymatou E, Vergara M R and Triantafyllidis T 2021a Effect of compaction banding on the hydraulic properties of porous rock: Part I – Experimental investigation; *Rock Mech. Rock Eng.* **54** 2671–2683, <https://doi.org/10.1007/s00603-021-02427-w>.
- Leuthold J, Gerolymatou E and Triantafyllidis T 2021b Effect of compaction banding on the hydraulic properties of porous rock – Part II: Constitutive description and numerical simulations; *Rock Mech. Rock Eng.* **54** 2685–2696, <https://doi.org/10.1007/s00603-021-02430-1>.
- Marketos G and Bolton M D 2009 Compaction bands simulated in discrete element models; *J. Struct. Geol.* **31(5)** 479–490.
- Matyka M, Khalili A and Koza Z 2008 Tortuosity-porosity relation in porous media flow; *Phys. Rev. E* **78(2)** 1–8.
- Menéndez B, Zhu W and Wong T-f 1996 Micromechanics of brittle faulting and cataclastic flow in Berea sandstone; *J. Struct. Geol.* **18(1)** 1–16.
- Morris J P, Lomov I N and Glenn L A 2003 A constitutive model for stress-induced permeability and porosity evolution of Berea sandstone; *J. Geophys. Res.: Solid Earth* **108(B10)**.
- Nanda K, Vaishakh T K, Das A and Misra S 2020 Hydro-mechanical response in porous rocks during localized deformation: Finite element analysis; *J. Struct. Geol.* **130**.
- Nguyen G D and Einav I 2009 The energetics of cataclasis based on breakage mechanics; *Pure Appl. Geophys.* **166(10)** 1693–1724.
- Nguyen V H, Gland N, Dautriat J, David C, Wassermann J and Guélard J 2014 Compaction, permeability evolution and stress path effects in unconsolidated sand and weakly consolidated sandstone; *Int. J. Rock Mech. Min. Sci.* **67** 226–239.
- Sari M, Sarout J, Poulet T, Dautriat J and Veveakis M 2022 The brittle–ductile transition and the formation of compaction bands in the Savonnières Limestone: Impact of the stress and pore fluid; *Rock Mech. Rock Eng.* **55** 6541–6553, <https://doi.org/10.1007/s00603-022-02963-z>.
- Sun W, Kuhn M R and Rudnicki J W 2013 A multiscale DEM-LBM analysis on permeability evolutions inside a dilatant shear band; *Acta Geotech.* **8** 465–480, <https://doi.org/10.1007/s11440-013-0210-2>.
- Vajdova V, Baud P and Wong T-f 2004 Permeability evolution during localized deformation in Bentheim sandstone; *J. Geophys. Res.* **109(B10)** B10406.
- Wang Q, Hu X, Zheng W, Li L, Zhou C, Ying C and Xu C 2021 Mechanical properties and permeability evolution of red sandstone subjected to hydro-mechanical coupling: Experiment and discrete element modelling; *Rock Mech. Rock Eng.* **54** 2405–2423, <https://doi.org/10.1007/s00603-021-02396-0>.
- Wong T and Baud P 2012 The brittle–ductile transition in porous rock: A review; *J. Struct. Geol.* **44** 25–53.
- Zhu W and Wong T-f 1997 The transition from brittle faulting to cataclastic flow: Permeability evolution; *J. Geophys. Res.* **102(B2)** 3027–3041.

Corresponding editor: SOMNATH DASGUPTA